RSC Advances

ROYAL SOCIETY OF CHEMISTRY

www.rsc.org/advances

Electrophoretic Deposited Oxide Thin Films as Charge Transporting Interlayers for Solution-Processed Optoelectronic Devices: the Case of ZnO Nanocrystals

Sai Bai,[a] Shasha He,[a] Yizheng Jin,[a *] Zhongwei Wu,[b] Zhouhui Xia,[b] Baoquan Sun,[b] Xin Wang,[a] Zhizhen Ye,[a] Feng Gao,[c] Shuyan Shao,[c] and Fengling Zhang[c]

[a] *State Key Laboratory of Silicon Materials, Center for Chemistry of High-Performance and Novel Materials, Cyrus Tang Center for Sensor Materials and Application, Department of Materials Science and Engineering, Zhejiang University, Hangzhou 310027, People's Republic of China*

[b] *Jiangsu Key Laboratory for Carbon-Based Functional Materials & Devices, Institute of Functional Nano & Soft Materials (FUNSOM), Soochow University, 199 Ren'ai Road, Suzhou 215123, People's Republic of China*

[c] *Biomolecular and Organic Electronics, IFM and Center of Organic Electronics, Linköping University SE-581 83 Linköping, Sweden*

Corresponding authors: Dr. Yizheng Jin (yizhengjin@zju.edu.cn)

Keywords: Electrophoretic deposition, ZnO nanocrystal, inverted organic solar cell, flexible optoelectronic device, polymer light emitting diode

Abstract: A promising fabrication method of electron transporting interlayers for solution-processed optoelectronic devices by electrophoretic deposition (EPD) of colloidal zinc oxide (ZnO) nanocrystals was demonstrated. A low voltage of 3-5 V and a short deposition time of 40 s at room temperature were found to be sufficient to generate dense and uniform ZnO thin films. The EPD ZnO nanocrystal films were applied as ETLs for inverted organic solar cell and polymer light emitting diodes (PLEDs). By optimizing the EPD processing of ZnO nanocrystal electron transporting layers (ETLs), inverted organic solar cells based on [3,4-b]-thiophene/benzodithiophene (PTB7): [6-6]-phenyl-C71-butyric acid methyl ester ($PC_{71}BM$) and poly(3-hexylthiophene) (P3HT): [6-6]-phenyl-C_{61}-butyric acid methyl ester ($PC_{61}BM$) with an average PCE of 8.4 % and 4.0% were fabricated. In combination with the PLEDs and flexible devices results, we conclude that the EPD processed ZnO nanocrystal thin films can serve as high quality ETLs for solution-processed optoelectronic devices.

Introduction

Solution-processed optoelectronic devices such as bulk-heterojunction (BHJ) solar cells, polymer light emitting diodes (PLEDs) and quantum dot light emitting diodes (QLEDs) offer low fabrication cost, large device area and physical flexibility due to the possibility of employing high throughput printing and coating techniques and the compatibility with plastic substrates.[1-6] Recently, low work function transition metal oxides including zinc oxide (ZnO) and titanium oxide (TiO_x) were introduced to modify the cathode as electron transporting layers (ETLs).[7-10] In addition, kinds of high work function metal oxides, such as molybdenum oxide (MoO_x), tungsten oxide (WO_x), vanadium oxide (VO_x) and nickel oxide (NiO_x) were employed as electron and hole transporting layers (HTLs) to modify the anodes of the solution-processed devices.[11-16] The use of metal oxide charge transporting layers (CTLs) led to devices with efficient charge extraction/injection characteristics and improved stability.

Employment of colloidal oxide nanocrystals, which decouples the synthesis of oxide crystals and the deposition of oxide thin films, is an attractive strategy for the fabrication of CTLs.[17-24] Advances in the synthetic chemistry of oxide nanocrystals enable fine tailoring of the band structures and electronic properties, which facilitate optimizing their electrical and interfacial properties of the CTLs.[25-30] In addition, colloidal nanocrystals can be readily integrated into devices by a variety of solution-based techniques owing to the excellent solution dispersibility.[31-36]

Among various solution-based techniques, electrophoretic deposition (EPD), a straightforward and versatile technique, may be one of the most promising approaches for future large-scale production of oxide nanocrystal thin films as CTLs for solution-processed devices. EPD offers unique combinations of cost effectiveness, long-range consistency in film thickness and surface morphology, size-scalability, high deposition rates, and site-selectivity.[37-39] Automated EPD processes have been widely used in industry for applying

coatings to electronics components, automobile parts and many other industrial products, shaping free-standing projects, the processing of advanced ceramic materials, and *etc.* Efforts of applying EPD for the fabrication of quantum dot sensitized solar cells, *i.e.* EPD of CdSe nanorods onto TiO_2 films, were reported.[40, 41] The Bulović´s group demonstrated the assembly of CdSe/ZnS quantum dots as emissive layers for QLEDs by EPD.[42] In contrast to spin coating, the most popular technique to deposit nanocrystal thin films in laboratory, EPD allows more efficient use of the starting nanocrystal solutions because majority of the nanocrystal solution is spun off the substrate and is wasted in the spin coating procedures. Herein we use EPD processed ZnO nanocrystal films as an example to demonstrate that EPD processed metal oxide nanocrystal thin films are highly desirable and beneficial for future industrial production of CTLs for solution-processed optoelectronic devices.

Experimental methods

Synthesis of ZnO nanocrystals. Colloidal ZnO nanocrystals were synthesized according to literature methods.[43, 44] All the chemical materials were purchased from Sigma-Aldrich and used as received. Typically, zinc acetate ($Zn(Ac)_2$, 819 mg, 4.46 mmol) was dissolved using 42 ml methanol in a three-necked flask. After heated to 60 ℃ under water bath, 250 μl of water was added into the solution. Methanol solution (23 ml) containing 7.72 mmol of potassium hydroxide (KOH, purity 85% +) was dropped into the flask within 8-10 min. The reacted solution was kept at 60 ℃ for 2.5 h. After washed by methanol for three times, the obtained ZnO nanocrystals were dissolved in a mixed solvent of chloroform and methanol (6 ml, 3:1 by volume) and filtered through 0.22 μm PTFE filters. The diameter of the nanocrystals was determined by dynamic light scattering measurements (Malvern, Nano-ZS90). The concentration of the resulting nanocrystal solution was measured by inductively coupled plasma atomic absorption spectrophotometer (ICP-AAS, Thermo Electron SOLAAR M6) to be 25 mg/ml.

EPD processed ZnO films. To conduct the EPD experiments, the ZnO nanocrystal solution was diluted to about 0.2 mg/ml by a mixed solvent of methanol and chloroform (4:1 by volume). A small amount of butylamine (40 μl) was introduced as capping ligands into 50ml diluted nanocrystal solution. Two ITO-coated glass substrates (4×1.5 cm^2 in size) parallel to each other with a gap of 5 cm were mounted into the diluted nanocrystal solution. The ITO substrates were cleaned by ultra-sonication in acetone, deionized water and ethanol, respectively and then treated by UV-ozone for 15min. A direct current (DC) voltage of 3-5 V was applied on the ITO electrodes for a desirable period. The spin-coated ZnO films were deposited by spin-coating the ZnO nanocrystal solution at 4000 rpm for 60 s. The resulted spin-coated and EPD ZnO thin films were transferred into a glove box and annealed at 150 ℃ for an hour to obtain full dense films. The obtained ZnO thin films were characterized by UV-visible absorption spectrum (Shimadzu UV 3600), atomic force microscopy (AFM, Veeco MultiMode V) and scanning electron microscopy (SEM, Hitachi SU70).

Device fabrication and characterization. For the poly(3-hexylthiophene) (P3HT): [6-6]-phenyl-C_{61}-butyric acid methyl ester ($PC_{61}BM$) solar cells, a solution of P3HT: $PC_{61}BM$ (1:0.8 by weight, 15 mg/ml) in 1, 2-dichlorobenzene was prepared by stirring for 12 h at 40 ℃. The blended solution was spin cast onto an EPD processed ZnO thin film at 700 rpm for 18 s. After the solvent slowly evaporated, the resulting active layer, ca. 180 nm in thickness, was annealed at 110 ℃ for 12 min in glove box. For the [3,4-b]-thiophene/benzodithiophene (PTB7): [6-6]-phenyl-C71-butyric acid methyl ester ($PC_{71}BM$) devices, the active layer (~80 nm) was prepared by spin-coating a mixed solvent of chlorobenzene/1,8-diiodoctane (97:3 % by volume) solution (1:1.5 by weight, 10 mg/ml) at 1000 rpm for 1min. Thin films of MoO_x (6 nm) and Al (100 nm) were deposited by thermal evaporation at a base pressure of 6 $\times 10^{-7}$ Torr. The active area of the devices, as defined by the overlapping of the aluminum and ITO electrodes, was 18.0 mm^2. Devices using spin-

coated ZnO nanocrystal thin films as electron-transporting interlayers with the same area were also fabricated under the same procedure as references. J-V characteristics were measured using Keithley 2400 source measure unit. Solar cell performance was characterized without encapsulation under ambient conditions using Newport Oriel xenon lamp (300 W) with an AM 1.5 filter. The light intensity was calibrated to 100 mW/cm2 using a Newport standard silicon solar cell 91150.

PLED devices were fabricated by spin-coating a solution of poly(9,9′-dioctylfluorene-co-benzothiadiazole) (F8BT) (12 mg/mL) in chlorobenzene to obtain thin films (80 nm). Bi-layer top electrodes of MoO_x/Al (20/100 nm) were deposited by thermal evaporation under a base pressure of 6×10^{-7} Torr. The device area was 3.24 mm^2 defined by the overlapping area of the ITO and top electrodes. For the PLED testing we used a Keithley 2400 electrometer for J-V characteristics and a fiber integration sphere (FOIS-1) couple with a QE-6500 spectrometer for light output measurements, as shown in Scheme S1.15 Note that the ITO glass substrate was in close contact with the input port of the integration sphere. The area of the PLED device was considerably smaller than that of the input port (9.5 mm in diameter) so that the PLED-to-integration sphere coupling factor was 1.

Results and discussion

The EPD experiments were conducted using butylamine capped ZnO nanocrystals. Fig. 1a shows the schematic of the EPD process. Typically, a low DC voltage of 3-5 V, which corresponds to an electric field of 0.6-1 V/cm, was applied to the ITO electrodes at room temperature under ambient conditions. Electrophoretic mobility measurements showed that the ZnO nanocrystals used in our experiments were positively charged and therefore only deposited onto the cathodes. The average diameter of the ZnO nanocrystals, determined by dynamic light scattering measurements, was around 5 nm. Fig. S1b reveals the UV-Vis absorption spectrum of the nanocrystal solution with butylamine ligands. The use of butylamine as capping ligands significantly improves the colloidal stability, leading to clear

solutions that can be stored under ambient conditions for several months. In contrast, a ligand-free ZnO nanocrystal solution generally became opalescent in a few days after preparation due to nanoparticles agglomeration (see Fig. S1c**)**. Therefore the capping ligands of butylamine are critical for practical applications. In addition, the introduction of butylamine dramatically increases the conductivity of the nanocrystal solutions by over one order of magnitude, from 6.8×10^{-3} to 9.8×10^{-2} mS/cm, partially due to the ionization of butylamine in the methanol containing solvent.[45] The influences of the addition of butylamine on the EPD processes and the resulting ZnO films will be discussed below.

Based on our current setup for the EPD experiments, a short deposition time of 40-200 s is sufficient to obtain high quality thin films with controllable thickness. A thin film deposited at 5 V for 120 s was used as an example to reveal the optical and morphological features of the EPD processed ZnO interlayers. Fig. 1b shows the top and cross-sectional views of the ZnO thin film, suggesting a uniform thickness of around 50 nm and the pinhole free feature. As illustrated by the transmittance spectra and the digital image shown in Fig. 1c, the EPD processed ZnO thin film is highly transparent in the visible region. The thickness of the ZnO nanocrystal films is readily tuned from 10±5 to 70±5 nm by controlling the processing parameters, e.g. the deposition time and the potential applied to the electrodes (Fig. 1d). The homogeneous surfaces of the thin films were also supported by the AFM measurements (Fig. 1e). The height profile of the AFM image indicates that the root mean square (RMS) surface height of the ZnO films was about 4.5 nm. The phase image exhibits almost no variations and there is no significant contrast in the optical image with a relative lower magnification (Fig S2), implying the uniform surface features of the EPD processed ZnO thin film.

Inverted organic solar cells were fabricated, demonstrating the availability of EPD ZnO films as ETLs for solution-processed optoelectronic devices. The device structure was shown in Fig. 2a. A model system of P3HT: $PC_{61}BM$ was used to study the correlation of the EPD processes and the OPV devices based on the resulting ZnO nanocrystal films. The

experimental parameters, including capping ligands and deposition time, as well as the performances of the devices are listed in Tab. S1. We found that the capping ligands of butylamine were critical for the EPD processes. Without the addition of butylamine, the deposition current during the EPD process was approximately one order of magnitude lower compared with that conducted with the butylamine capped ZnO nanocrystals (Fig. S3a). The lower deposition current implied a significantly reduced deposition rate of the ZnO nanocrystals onto the ITO substrates. If a same deposition time (120 s, experiments 1 and 2 in Tab. S1) was applied, an incomplete covering of the ZnO nanocrystals was identified, as evidenced by a discontinuous phase image from the AFM measurements on the corresponding nanocrystal thin films (see Fig. S3b in Supporting Information). The incomplete covering of the ZnO nanocrystals led to devices exhibiting poor PCEs and larger reverse saturated dark current (Fig. S3c and S3d in Supporting Information). Once a complete covering of ZnO nanocrystals was achieved, the thickness of the ZnO nanocrystal thin films did not significantly affect the efficiencies of the devices. For the experiments conducted at the identical voltage (5 V, experiments 1 and 3-5 in Tab. S1), uniform ZnO nanocrystal films with thicknesses ranging from 15±5 to 70±5 nm were achieved by varying the deposition time from 40 to 200 s. The standard deviation figures (Fig. S4) of the device parameters show that for continuous ZnO nanocrystal films, a thickness of ~15 nm is sufficient to improve the contact properties of the ITO substrates. However, further increasing the deposition time to 300 s (experiment 6, Tab. S1) resulted in poor film morphologies including large clumps and particulates on the surfaces and degradation of the obtained devices. (Fig S4c) We noted that a few groups reported EPD processing of ZnO nanocrystals films before.[46-49] However, compared with the ZnO nanocrystal films obtained in our work, the films in those studies were in the micron-range, which were not suitable for ETLs applications. Our results also reveal the importance of optimizing the EPD processes, which are critical to achieve high quality CTLs and high performances devices.

The current density versus voltage (J-V) curves of the optimized devices using EPD processed ZnO ETLs and the reference devices based on spin-coated ZnO thin films with an identical thickness of 40 nm are shown in Fig. 2b. A decent average PCE of 4.0 % was achieved for P3HT: $PC_{61}BM$ devices with EPD processed ZnO ETLs. The parameters of open circuit voltage (V_{OC}), short circuit current (J_{SC}) and fill factor (FF) are all comparable to the reference devices with spin-coated ZnO ETLs, as shown in Tab. 1. We compared the ZnO nanocrystal ETLs fabricated by EPD or spin-coating. The AFM image and the transmittance spectrum of the spin-coated ZnO films are shown in Figure S5. The results show that the RMS of surface height (4.2 nm) and the transparency of the EPD processed ZnO films are comparable to those of the spin-coated ZnO films. We note that spin coating is a rapid film-forming process while EPD is a much gentler and slower deposition method. EPD may lead to ZnO films with more energetically favorable packing of nanocrystals and thereby better performance of the solar cells with EPD processed ZnO ETLs.

We suggest that the EPD approach is ideal for flexible electronics applications, owing to two key advantages of this technique: room temperature deposition and no restriction on the shape and nature of the substrates. EPD of ZnO nanocrystals onto the ITO/polyethylene-naphthalate (PEN) substrates were conducted and flexible inverted P3HT: $PC_{61}BM$ solar cells were fabricated (Fig. 2c). An impressive average PCE of 3.7% was achieved, demonstrating the compatibility of the EPD processes with flexible substrates.

We also applied the optimized EPD processed ZnO ETLs to the inverted organic solar cells using blends of PTB7: $PC_{71}BM$. The J-V curves under illumination and dark are shown in Fig. 3a, b. The devices based on EPD ZnO interlayers exhibited an average PCE of 8.4 % and a champion PCE of 8.6% with a J_{SC} of 16.05 mA cm^{-2}, a V_{OC} of 0.74 V and a high FF of 0.73, which was similar with the device based on spin-coated ZnO ETLs. The detailed device characteristics are summarized in Tab. 2. The external quantum efficiency (EQE) spectra for the solar cells are illustrated in Fig. 3c. Integrating the EQE data gives a short circuit current

of 15.59 and 15.93 mA cm^{-2} for devices based on EPD and spin coated ZnO film, which is about ~3 % difference from the values measured. These results show that the EPD deposited ZnO nanocrystal ETLs are favorable candidates for high efficiency organic solar cells.

Upon successful efforts on the inverted organic solar cells, we further applied the EPD processed ZnO nanocrystal thin films to inverted PLED devices using F8BT as the emitter. The device structure and the characteristics of current density versus voltage (J-V) and luminance versus voltage are shown in Fig. 4. The inset in Fig. 4b shows the plots of EQE versus voltage. The devices based on EPD processed ZnO ETLs exhibited a brightness of 67144 cd/m^2 at 7 V and a maximum EQE value of 1.02 %. Both the efficiency and brightness of the devices using EPD processed ZnO thin films were slightly improved in comparison with the devices based on spin-coated ZnO films. The results indicate that the EPD ZnO films are also favorable candidates as ETLs for PLEDs.

Conclusions

In short, we demonstrated the fabrication of ETLs for solution-processed optoelectronic devices by EPD of colloidal ZnO nanocrystals. The EPD processes were conducted at room temperature under ambient conditions. The use of butylamine ligands was critical in terms of improving the colloidal stability of the nanocrystal solutions and regulating the EPD processes. We found that a low DC potential of 3-5 V and a short deposition time of 40-200 s is sufficient to generate compacted and uniform ZnO thin films with excellent visible transparency and controllable thickness. Optimizing the EPD processing of ZnO nanocrystal ETLs led to inverted organic solar cells based on PTB7: $PC_{71}BM$ and P3HT: $PC_{61}BM$ with an average PCE of 8.4 % and 4.0%, respectively. We also demonstrate that the EPD ZnO nanocrystal ETLs are compatible with flexible substrates. In combination with the PLED results, we conclude that the EPD processed ZnO nanocrystal thin films, which are compatible with flexible substrates, can serve as high quality ETLs for solution-processed

optoelectronic devices. The EPD approach may be extended to the deposition of other oxide nanocrystal thin films and the fabrication of CTLs. Considering the advantages of EPD processes, the low applied voltage and short deposition time used in our experiments and the advances on the synthetic chemistry of colloidal oxide nanocrystals, our study provides a promising method to fabricate oxide CTLs for solution-processed optoelectronic devices at industrial scale.

Acknowledgements

This work is financially supported by the National High Technology Research and Development Program of China (2011AA050520), the National Basic Research Program of China (973 Program, 2012CB932402), the National Natural Science Foundation of China (51172203), Natural Science Funds for Distinguished Young Scholar of Zhejiang Province (R4110189) and the Public Welfare Project of Zhejiang Province (2013C31057). Financial supports from Swedish Energy Agency (Energimyndigheten) and the Swedish Research Council (VR) are also greatly appreciated.

Notes and references

1 G. Yu, J. Gao, J. C. Hummelen, F. Wudl, A. J. Heeger, *Science* 1995, **270**, 1789.

2 X. Dai, Z. Zhang, Y. Jin, Y. Niu, H. Cao, X. Liang, L. Chen, J. Wang, X. Peng, *Nature* 2014, **515**, 96.

3 D. Kabra, L. P. Lu, M. H. Song, H. J. Snaith, R. H. Friend, *Adv. Mater.* 2010, **22**, 3194.

4 L. Qian, Y. Zheng, J. Xue, P. H. Holloway, *Nat. Photonics* 2011, **5**, 543.

5 J. Y. Kim, K. Lee, N. E. Coates, D. Moses, T. Q. Nguyen, M. Dante, A. J. Heeger, *Science* 2007, **317**, 222.

6 O. Inganäs, F. Zhang, K. Tvingstedt, L. M. Andersson, S. Hellström, M. R. Andersson, *Adv. Mater.* 2010, **22**, E100.

7 Z. Ma, Z. Tang, E. Wang, M. R. Andersson, O. Inganäs, F. Zhang, *J. Phys. Chem. C* 2012, **116**, 24462.

8 S. Bai, Z. Wu, X. Xu, Y. Jin, B. Sun, X. Guo, S. He, X. Wang, Z. Ye, H. Wei, X. Han, W. Ma, *Appl. Phys. Lett.* 2012, **100**, 203906.

9 Y. Sun, J. H. Seo, C. J. Takacs, J. Seifter, A. J. Heeger, *Adv. Mater.* 2011, **23**, 1679.

10 J. Y. Kim, S. H. Kim, H. H. Lee, K. Lee, W. Ma, X. Gong, A. J. Heeger, *Adv. Mater.* 2006, **18**, 572.

11 J. Meyer, S. Hamwi, M. Kröger, W. Kowalsky, T. Riedl, A. Kahn, *Adv. Mater.* 2012, **24**, 5408.

12 T. Stubhan, N. Li, N. A. Luechinger, S. C. Halim, G. J. Matt, C. J. Brabec, *Adv. Energy Mater.* 2012, **2**, 1433.

13 K. Zilberberg, S. Trost, J. Meyer, A. Kahn, A. Behrendt, D. Lützenkirchen Hecht, R. Frahm, T. Riedl, *Adv. Funct. Mater.* 2011, **21**, 4776.

14 K. X. Steirer, P. F. Ndione, N. E. Widjonarko, M. T. Lloyd, J. Meyer, E. L. Ratcliff, A. Kahn, N. R. Armstrong, C. J. Curtis, D. S. Ginley, J. J. Berry, D. C. Olson, *Adv. Energy Mater.* 2011, **1**, 813.

15 S. Bai, M. Cao, Y. Jin, X. Dai, X. Liang, Z. Ye, M. Li, J. Cheng, X. Xiao, Z. Wu, Z. Xia, B. Sun, E. Wang, Y. Mo, F. Gao, F. Zhang, *Adv. Energy Mater.* 2014**,** 4, 1301460

16 J. R. Manders, S.W. Tsang, M. J. Hartel, T. H. Lai, S. Chen, C. M. Amb, J. R. Reynolds, F. So, *Adv. Funct. Mater.* 2013, **23**, 2993.

17 S. Chen, C. E. Small, C. M. Amb, J. Subbiah, T. h. Lai, S.W. Tsang, J. R. Manders, J. R. Reynolds, F. So, *Adv. Energy Mater.* 2012, **2**, 1333.

18 J. You, C. C. Chen, L. Dou, S. Murase, H. S. Duan, S. A. Hawks, T. Xu, H. J. Son, L. Yu, G. Li, Y. Yang, *Adv. Mater.* 2012, **24**, 5267.

19 S. K. Hau, H. L. Yip, N. S. Baek, J. Zou, K. O'Malley, A. K. Y. Jen, *Appl. Phys. Lett.* 2008, **92**, 253301.

20 J. Meyer, R. Khalandovsky, P. Görrn, A. Kahn, *Adv. Mater.* 2011, **23**, 70.

21 T. Stubhan, T. Ameri, M. Salinas, J. Krantz, F. Machui, M. Halik, C. J. Brabec, *Appl. Phys. Lett.* 2011, **98**, 253308.

22 Y. J. Lee, J. Yi, G. F. Gao, H. Koerner, K. Park, J. Wang, K. Luo, R. A. Vaia, J. W. P. Hsu, *Adv. Energy Mater.* 2012, **2**, 1193.

23 S. Bai, Y. Jin, X. Liang, Z. Ye, Z. Wu, B. Sun, Z. Ma, Z. Tang, J. Wang, U. Würfel, F. Gao, F. Zhang, *Adv. Energy Mater.* 2014, DOI:10.1002/aenm.201401606

24 X. Liang, Q. Yi, S. Bai, X. Dai, X. Wang, Z. Ye, F. Gao, F. Zhang, B. Sun, Y. Jin, *Nano Lett.* 2014, **14**, 3117.

25 A. W. Cohn, K. R. Kittilstved, D. R. Gamelin, *J. Am. Chem. Soc.* 2012, **134**, 7937.

26 Y. Yang, Y. Jin, H. He, Q. Wang, Y. Tu, H. Lu, Z. Ye, *J. Am. Chem. Soc.* 2010, **132**, 13381.

27 X. Wang, Y. Jin, H. He, F. Yang, Y. Yang, Z. Ye, *Nanoscale* 2013, **5**, 6464.

28 Y. Jin, Q. Yi, L. Zhou, D. Chen, H. He, Z. Ye, J. Hong, C. Jin, *Eur. J. Inorg. Chem.* 2012, **2012**, 4268.

29 R. Buonsanti, A. Llordes, S. Aloni, B. A. Helms, D. J. Milliron, *Nano Lett.* 2011, **11**, 4706.

30 E. Della Gaspera, M. Bersani, M. Cittadini, M. Guglielmi, D. Pagani, R. Noriega, S. Mehra, A. Salleo, A. Martucci, *J. Am. Chem. Soc.* 2013, **135**, 3439.

31 M. Boberl, M. V. Kovalenko, S. Gamerith, E. J. W. List, W. Heiss, *Adv. Mater.* 2007, **19**, 3574.

32 D. V. Talapin, J. S. Lee, M. V. Kovalenko, E. V. Shevchenko, *Chem. Rev.* 2009, **110**, 389.

33 D. V. Talapin, C. B. Murray, *Science* 2005, **310**, 86.

34 P. O. Anikeeva, J. E. Halpert, M. G. Bawendi, V. Bulović, *Nano Lett*. 2009, **9**, 2532.

35 M. I. Bodnarchuk, M. V. Kovalenko, S. Pichler, G. Fritz-Popovski, G. Hesser, W. Heiss, *ACS Nano* 2010, **4**, 423.

36 K. ul Hasan, O. Nur, M. Willander, *Appl. Phys. Lett*. 2012, **100**, 211104

37 O. O. Van der Biest, L. J. Vandeperre, *Annu. Rev. Mater. Sci.* 1999, **29**, 327.

38 P. Sarkar, P. S. Nicholson, *J. Am. Ceram. Soc.* 1996, **79**, 1987.

39 M. Ammam, *RSC Advances* 2012, **2**, 7633.

40 A. Salant, M. Shalom, I. Hod, A. Faust, A. Zaban, U. Banin, *ACS Nano* 2010, **4**, 5962.

41 A. Salant, M. Shalom, Z. Tachan, S. Buhbut, A. Zaban, U. Banin, *Nano Lett.* 2012, **12**, 2095.

42 K. W. Song, R. Costi, V. Bulović, *Adv. Mater.* 2013, **25**, 1420.

43 B. Sun, H. Sirringhaus, *Nano Lett.* 2005, **5**, 2408.

44 Y. Jin, J. Wang, B. Sun, J. C. Blakesley, N. C. Greenham, *Nano Lett.* 2008, **8**, 1649.

45 J. R. Schaefgen, M. S. Newman, F. H. Verhoek, *J. Am. Chem. Soc.* 1944, **66**, 1847.

46 E. M. Wong, P. C. Searson, *Appl. Phys. Lett.* 1999, **74**, 2939.

47 M. Verde, M. Peiteado, A. C. Caballero, M. Villegas, B. Ferrari, *J. Colloid Interface Sci.* 2012, **373**, 27.

48 Y. C. Wang, I. C. Leu, M. H. Hon, *J. Am. Ceram. Soc.* 2004, **87**, 84.

49 L. Miao, S. Cai, Z. Xiao, *J. Alloys Compd.* 2010, **490**, 422.

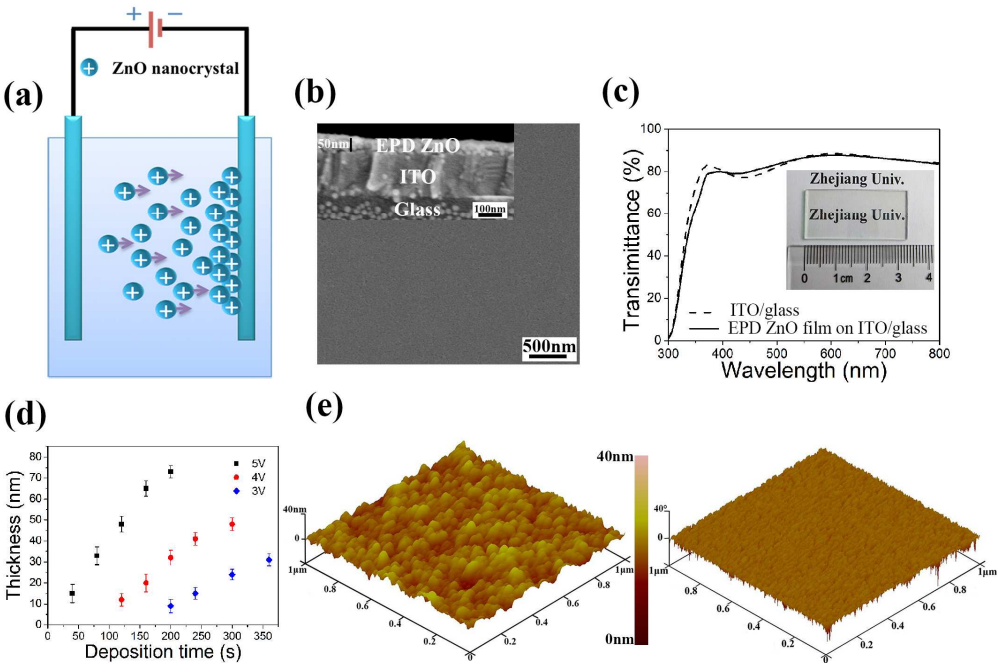

Fig. 1 a) Schematic of the electrophoretic deposition process of ZnO nanocrystal films. b) Top view and the cross-sectional (inset) SEM image of the annealed EPD processed ZnO film. c) Transmittance spectra of the EPD ZnO nanocrystal film on ITO/glass substrate and the ITO/glass substrate. The inset shows a digital picture of the EPD ZnO nanocrystal film. d) The obtained film thickness versus deposition time of the EPD processes at different applied voltages. e) 3D height profile and the corresponding phase image of the EPD processed ZnO nanocrystal film deposited at 5 V for 120 s.

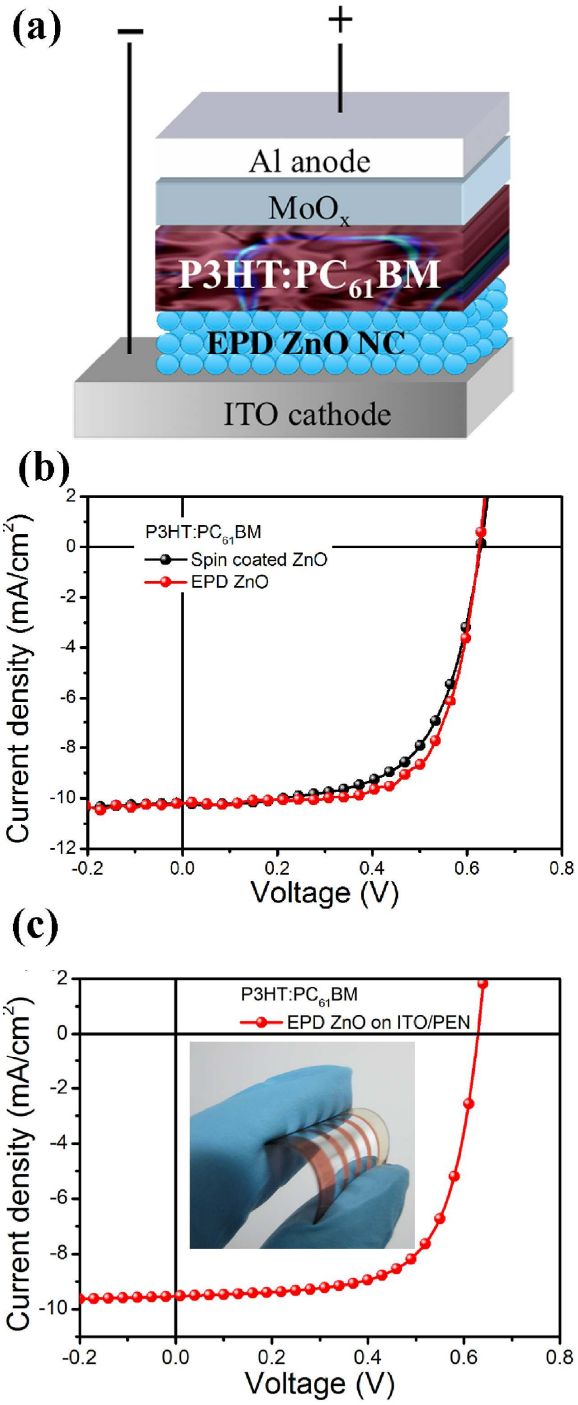

Fig. 2 a) Device structure of the inverted organic solar cell. b) J-V characteristics of the inverted P3HT: $PC_{61}BM$ solar cells based on EPD ZnO nanocrystal film on ITO/glass substrates and the control device based on spin coated ZnO interlayer on the ITO/glass substrate, respectively. c) J-V curve of flexible ITO/ PEN device. Inset: photograph of the plastic solar cell based on EPD ZnO film.

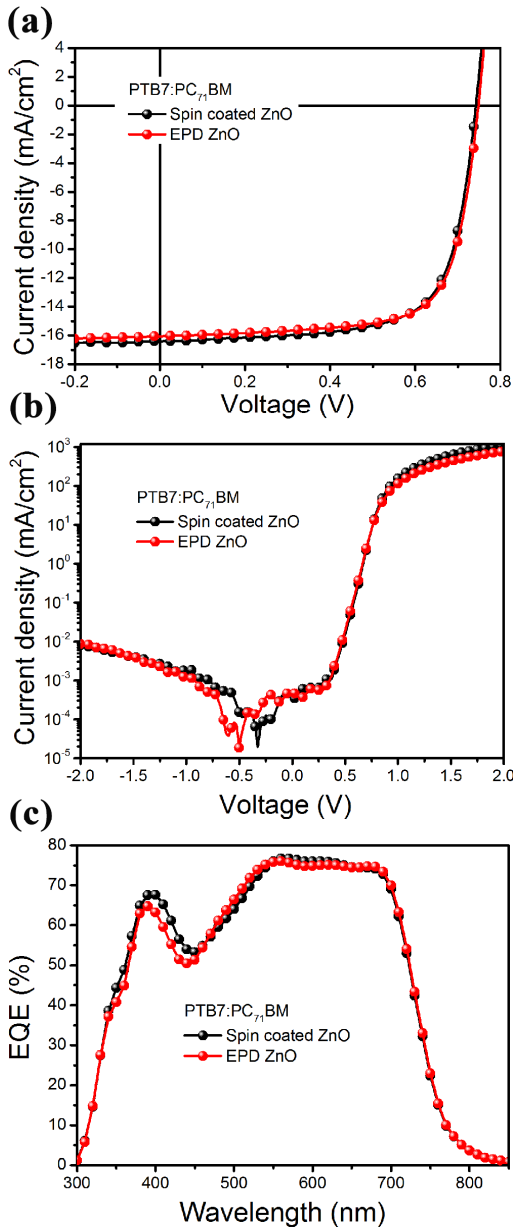

Fig. 3 Inverted PTB7: $PC_{71}BM$ solar cells with EPD processed ZnO nanocrystal ETLs and the reference devices with spin-coated ZnO nanocrystal ETLs. a) Light J-V, b) dark J-V characteristics and c) EQE spectra.

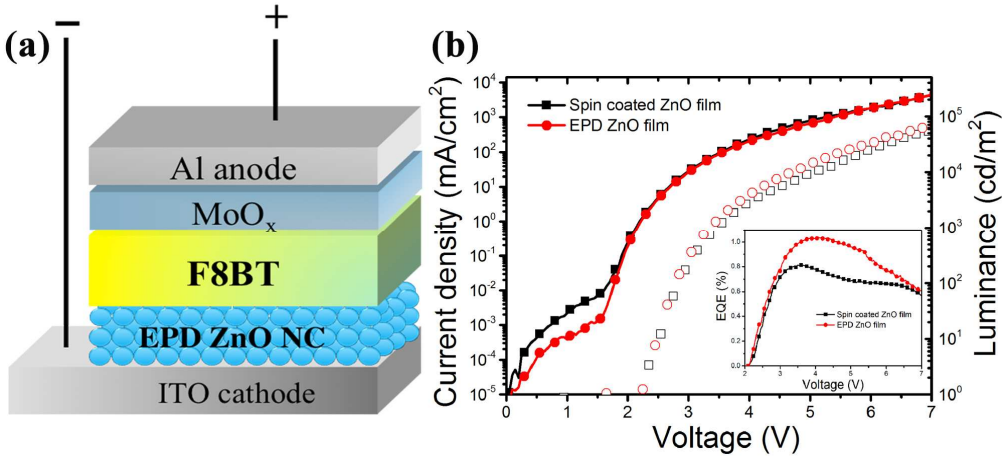

Fig. 4 PLEDs using EPD ZnO nanocrystal films and spin-coated ZnO films as the ETLs. (a) Device structure. (b) Curves of current density and luminance versus applied bias of two devices. The inset shows the EQE curves as a function of the applied bias.

Tab. 1 Device performance parameters of inverted organic solar cells based on P3HT:$PC_{61}BM$ with the reference spin-casted ZnO films (SP-ZnO) and optimized EPD processed ZnO films (EPD-ZnO) as the ETLs.

Device	V_{OC} **(V)**	J_{SC} **(mA cm^{-2})**	***FF***	**Best *PCE* (%)**	**Average *PCE* (%)**
P3HT:$PC_{61}BM$ on SP-ZnO	0.62	10.27	0.64	4.07	3.8 ± 0.2
P3HT:$PC_{61}BM$ on EPD-ZnO	0.62	10.08	0.68	4.24	4.0 ± 0.2
P3HT:$PC_{61}BM$ on EPD-ZnO/PEN	0.62	9.54	0.67	3.96	3.7 ± 0.2

Tab. 2 Device performance parameters of inverted PTB7:$PC_{71}BM$ organic solar cells with SP-ZnO and optimized EPD-ZnO films as the ETLs.

Device	V_{OC} **(V)**	J_{SC} **(mA cm^{-2})**	***FF***	**Best *PCE* (%)**	**Average *PCE* (%)**
PTB7:$PC_{71}BM$ on SP-ZnO	0.74	16.39	0.71	8.57	8.3 ± 0.2
PTB7:$PC_{71}BM$ on EPD-ZnO	0.74	16.05	0.73	8.66	8.4 ± 0.2

Tab. 3 Device parameters of the PLEDs based on F8BT using EPD-ZnO and spin-coated SP-ZnO interlayers as ETLs.

ETLs	V_{on} (V)	Maximum L_V (cd m^{-2})	Maximum EQE
SP-ZnO	2.2	55482	0.81
EPD-ZnO	2.2	67144	1.02

ToC figure

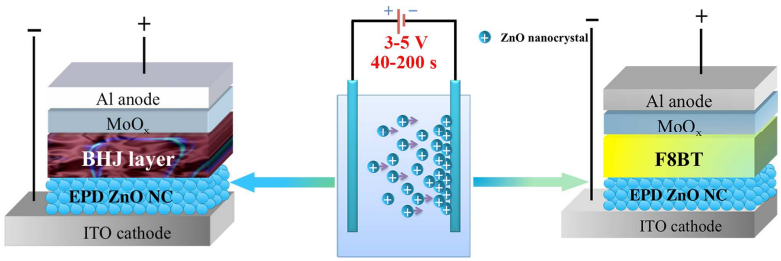

Supporting Information

Electrophoretic Deposited Oxide Thin Films as Charge Transporting Interlayers for Solution-Processed Optoelectronic Devices: the Case of ZnO Nanocrystals

Sai Bai,[a] Shasha He,[a] Yizheng Jin,[a,b,c] Zhongwei Wu,[d] Baoquan Sun,[d] Xin Wang,[a] Zhizhen Ye,[a,b] Feng Gao,[e] Shuyan Shao,[e] and Fengling Zhang [e]*

[a] State Key Laboratory of Silicon Materials, Department of Materials Science and Engineering, Zhejiang University, Hangzhou 310027, People's Republic of China
[b] Cyrus Tang Center for Sensor Materials and Applications, Zhejiang University Hangzhou 310027, People's Republic of China
[c] Center for Chemistry of High-Performance and Novel Materials, Zhejiang University, Hangzhou 310027, People's Republic of China
[d] Jiangsu Key Laboratory for Carbon-Based Functional Materials & Devices, Institute of Functional Nano & Soft Materials (FUNSOM), Soochow University, 199 Ren'ai Road, Suzhou 215123, People's Republic of China
[e] Biomolecular and Organic Electronics, IFM and Center of Organic Electronics, Linköping University SE-581 83 Linköping, Sweden

Corresponding authors: Dr. Yizheng Jin (yizhengjin@zju.edu.cn)

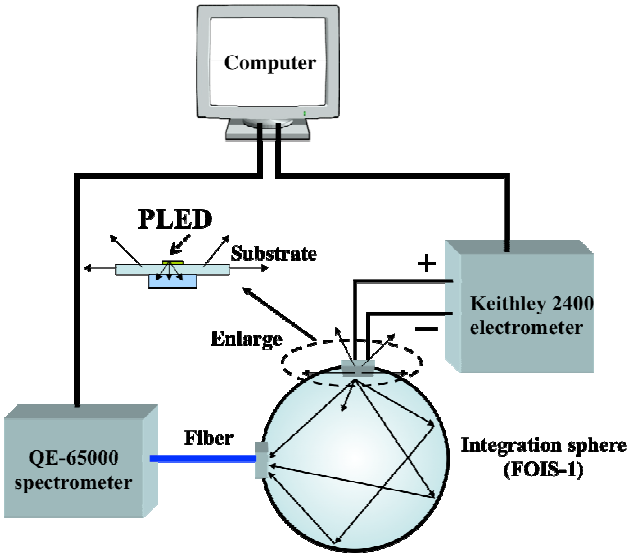

Scheme S1. PLED measurement system.

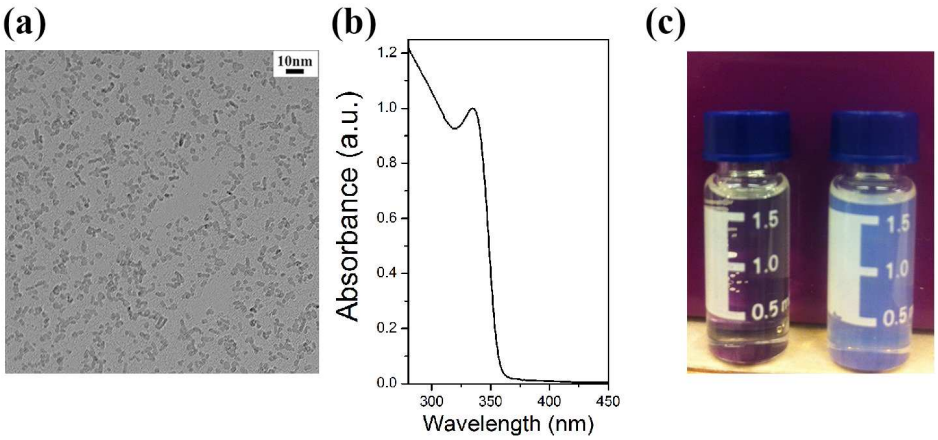

Fig. S1 a) A typical TEM image of colloidal ZnO nanocrystals. b) Absorption spectrum of the ZnO nanocrystal solution. c) Digital pictures of the nanocrystal solution with (left) and without butylamine ligand (right) stored under ambient conditions for 60 and 10 days, respectively.

Fig. S2 Optical image of 1 mm^2 area EPD ZnO film obtained at 5V for 120 s.

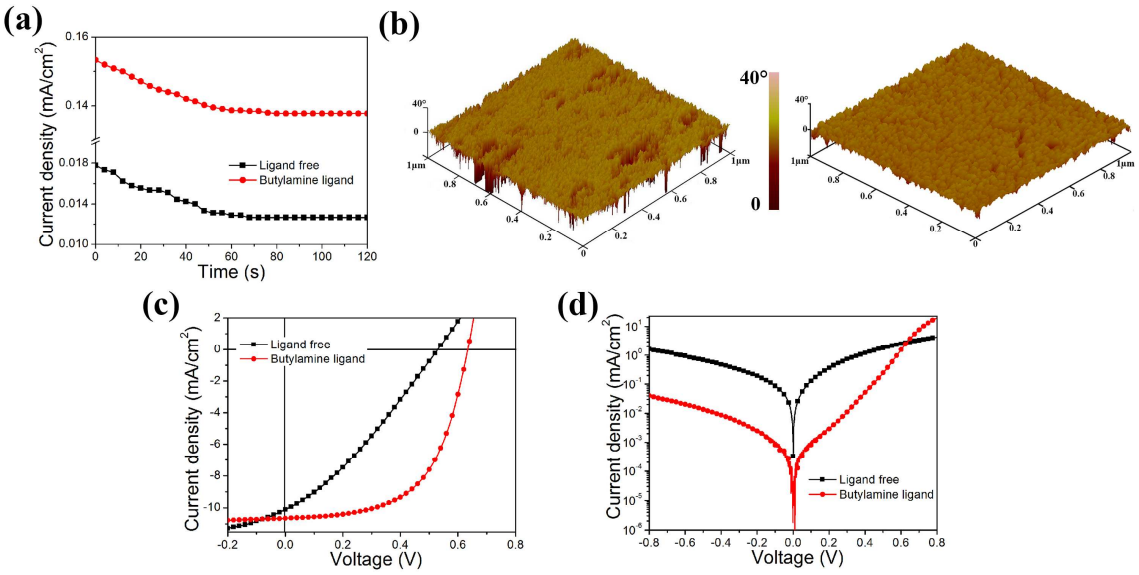

Fig. S3 a) Current density versus time during the EPD experiments of ZnO nanocrystal solution. b) 3D AFM phase images of EPD processed ZnO nanocrystal films obtained from the solution without ligand (left) and with butylamine as capping ligand (right) under the same applied voltage, respectively. c) and d) J-V curves of inverted P3HT: $PC_{61}BM$ solar cells fabricated on EPD ZnO films (both with and without butylamine ligands) under illumination and dark, respectively.

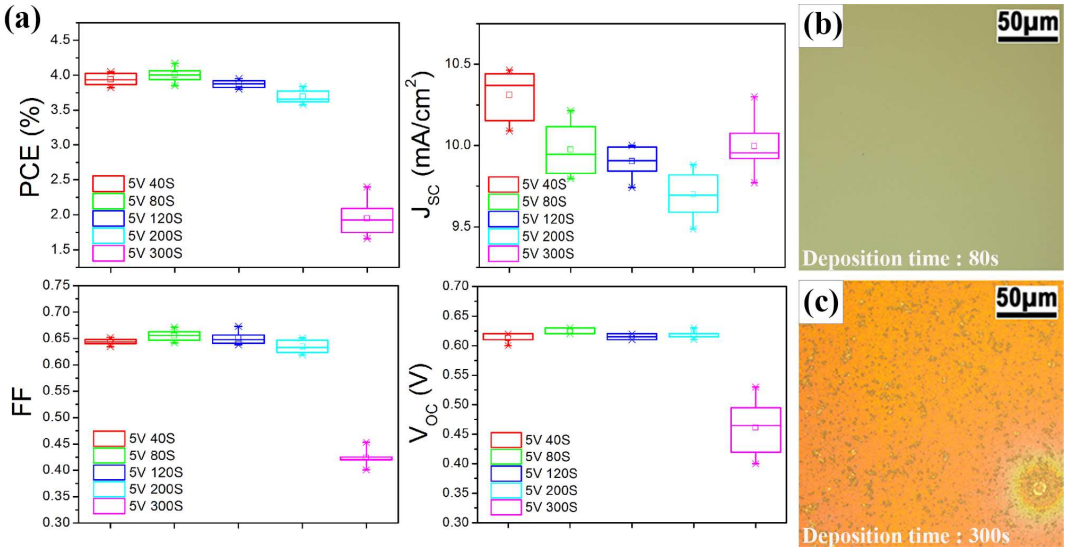

Fig. S4 a) Standard deviation profiles for all device parameters of the inverted organic solar cells based on the analysis of ten devices with EPD processed ZnO interlayers deposited from different deposition time. b) and c) Optical images of EPD processed ZnO interlayers obtained from different deposition time under 5 V applied voltage.

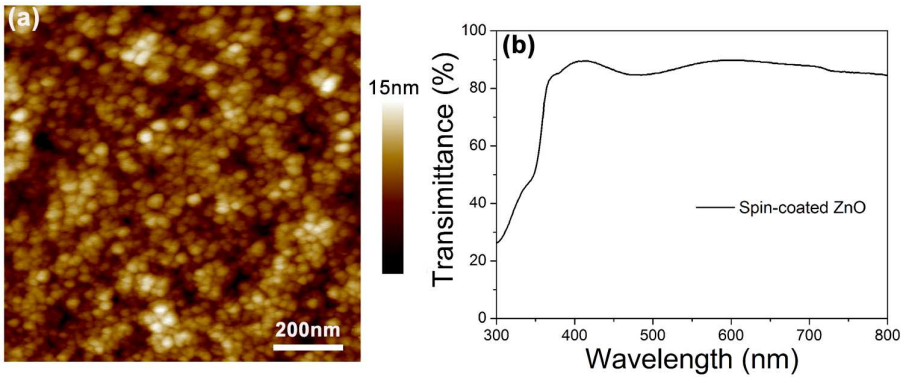

Fig. S5 Typical ZnO thin films obtained by spin-coating at 4000 rpm using a nanocrystal solution with chloroform and methanol as the solvent. a) AFM image and b) transmittancce spectrum on ITO substrate.

Tab. S1 Summary of processing parameters and the performance of inverted P3HT: $PC_{61}BM$ solar cells based on the EPD processed ZnO interlayers.

Experiment No.	**EPD parameters**	**Butylamine Ligands**	**Average *PCE* (%)**	**Best *PCE* (%)**
1	5 V，120 s	Yes	4.04	4.24
2	5 V，120 s	No	1.53	1.65
3	5 V，40 s	Yes	3.90	4.05
4	5 V，80 s	Yes	4.02	4.19
5	5 V，200 s	Yes	3.64	3.84
6	5 V，300 s	Yes	1.83	2.15